Dramatic reduction in dark current of β-Ga_2O_3 ultraviolet photodectors via β-$(Al_{0.25}Ga_{0.75})_2O_3$ surface passivation

Jian-Ying Yue(岳建英)[1,2], Xue-Qiang Ji(季学强)[1,2], Shan Li(李山)[1,2], Xiao-Hui Qi(岐晓辉)[1,2], Pei-Gang Li(李培刚)[1,2,†], Zhen-Ping Wu(吴真平)[1,2], and Wei-Hua Tang(唐为华)[1,2,3,‡]

[1] *Laboratory of Optoelectronics Materials and Devices, School of Science, Beijing University of Posts and Telecommunications, Beijing* 100876, *China*
[2] *State Key Laboratory of Information Photonics and Optical Communications, Beijing University of Posts and Telecommunications, Beijing* 100876, *China*
[3] *College of Electronic and Optical Engineering & College of Microelectronics, National and Local Joint Engineering Laboratory for RF Integration and Micro-Packaging Technologies, Nanjing University of Posts and Telecommunications, Nanjing* 210046, *China*

(Received 11 June 2022; revised manuscript received 15 August 2022; accepted manuscript online 18 August 2022)

Solar-blind ultraviolet photodetectors with metal-semiconductor-metal structure were fabricated based on β-$(Al_{0.25}Ga_{0.75})_2O_3/\beta$-$Ga_2O_3$ film grown by metal-organic chemical vapor deposition. It was known that various surface states increase dark current and a large number of defects can hinder the transport of carriers, resulting in low switching ratio and low responsivity of the device. In this work, β-$(Al_{0.25}Ga_{0.75})_2O_3$ films are used as surface passivation materials. Owning to its wide band gap, we obtain excellent light transmission and high lattice matching with β-Ga_2O_3. We explore the change and mechanism of the detection performance of the β-Ga_2O_3 detector after β-$(Al_{0.25}Ga_{0.75})_2O_3$ surface passivation. It is found that under the illumination with 254 nm light at bias 5 V, the β-$(Al_{0.25}Ga_{0.75})_2O_3/\beta$-$Ga_2O_3$ photodetectors show dark current of just 18 pA and high current on/off ratio of 2.16×10^5. The dark current is sharply reduced about 50 times after passivation of the β-Ga_2O_3 surface, and current on/off ratio increases by approximately 2 times. It is obvious that β-Ga_2O_3 detectors with β-$(Al_{0.25}Ga_{0.75})_2O_3$ surface passivation can offer superior detector performance.

Keywords: β-$(Al_{0.25}Ga_{0.75})_2O_3/\beta$-$Ga_2O_3$, MOCVD, photodetectors, defect passivation

PACS: 67.30.hr, 71.20.Nr, 85.60.Gz, 81.65.Rv **DOI:** 10.1088/1674-1056/ac8a8e

1. Introduction

It is well known that β-Ga_2O_3 is a new type of ultra-wide band gap semiconductor material. Compared with SiC and GaN, the band gap of β-Ga_2O_3 reaches 4.9 eV, which is higher than 3.25 eV of SiC and 3.4 eV of GaN.[1–4] Due to its anti-irradiation and high temperature resistance, it can maintain stable properties in extreme environments such as high and low temperature and strong radiation, and its high breakdown field strength ensures that a prepared β-Ga_2O_3 device can be used under ultra-high voltage, which is beneficial to improve the carrier collection efficiency.[5,6] Based on these, power devices based on β-Ga_2O_3 are expected to have higher breakdown voltage and lower on-resistance, resulting in lower conduction losses and higher power conversion efficiency.[7] These characteristics ensure that β-Ga_2O_3 is promising to applications in the field of power electronics devices. Furthermore, β-Ga_2O_3 is an ideal candidate for solar-blind ultraviolet (UV) detection due to its wide band gap, large UV absorption coefficient, and easy processing, etc.[8,9]

As we know, wide-bandgap β-$(Al_xGa_{1-x})_2O_3$ films would enable higher critical field strength in power electronic devices.[10] Entry of Al elements can effectively modulate the band gap of intrinsic β-Ga_2O_3. For example, a β-$(Al_xGa_{1-x})_2O_3$ film can adjust the band gap and carrier concentration.[11–13] Also, β-$(Al_xGa_{1-x})_2O_3$ film can be employed in modulation-doped β-$(Al_xGa_{1-x})_2O_3/\beta$-$Ga_2O_3$ heterostructures, where the separation between the ionized donor impurities and the two-dimensional electron gas would enable higher electron mobilities.[14] Various methods for growth of β-$(Al_xGa_{1-x})_2O_3$ films have been explored, such as molecular beam epitaxy (MBE), pulsed laser deposition (PLD),[15] metal organic chemical vapor deposition (MOCVD),[16] and magnetron sputtering.[17] The earliest documents indicate that, in 2012, Ito *et al.*[18] used the mist-CVD method to deposit and grow α-$(AlGa)_2O_3$ thin films. In recent years, Miller *et al.* used TEAl and TMAl as Al sources to perform MOCVD deposition of β-$(Al_{0.21}Ga_{0.79})_2O_3/Ga_2O_3$ film superlattice structure.[16] Although the β-$(Al_xGa_{1-x})_2O_3$ films have received a certain degree of widespread attention, there are few reports on preparation of detectors for passivating β-Ga_2O_3 film surfaces with β-$(Al_xGa_{1-x})_2O_3$ films.

In this work, we adjust the ratio of [TMAl]/[TMAl + TEGa] by adjusting the amount of injected TMAl flow, to obtain β-$(Al_xGa_{1-x})_2O_3/\beta$-$Ga_2O_3$ films at $x = 24.71\%$. Moreover, the β-$(Al_{0.25}Ga_{0.75})_2O_3$ films are used as surface passivation materials due to their wider band width and excellent optical transmittance. The MOCVD epitaxy only needs to cut into the TMAl source to continuously grow without taking out the chamber and then to coat the film with plasma enhanced chemical vapor deposition (PECVD) or other coating equip-

†Corresponding author. E-mail: pgli@bupt.edu.cn
‡Corresponding author. E-mail: whtang@njupt.edu.cn

© 2023 Chinese Physical Society and IOP Publishing Ltd

ment, for simultaneously reducing air water oxygen pollution, achieving high quality interfacial continuation, reducing surface defects and high lattice match with β-Ga_2O_3. We explore the change and mechanism of detection performance of the β-Ga_2O_3 film detector after β-$(Al_{0.25}Ga_{0.75})_2O_3$ surface passivation. It is found that under illumination with 254 nm light at bias 5 V, the β-$(Al_{0.25}Ga_{0.75})_2O_3/\beta$-$Ga_2O_3$ photodetectors (PDs) show low dark current and high current on/off ratio, the dark current is sharply reduced by about 50 times after passivation of the β-Ga_2O_3 surface, and current on/off ratio increases by approximately 2 times. The results show that β-Ga_2O_3 detectors with β-$(Al_{0.25}Ga_{0.75})_2O_3$ surface passivation offer superior detector performance and β-$(Al_{0.25}Ga_{0.75})_2O_3$ has great potential applications as a passivation material in the field of ultraviolet photoelectric detection.

2. Experiment

In experiment, we investigated growth of $(\bar{2}01)$ β-$(Al_{0.25}Ga_{0.75})_2O_3/\beta$-$Ga_2O_3$ films on (0001)-oriented sapphire with a low-temperature β-Ga_2O_3 buffer at 630 °C using a closed-coupled showerhead-MOCVD (CCS-MOCVD). Triethylgallium (TEGa,6N) and trimethylaluminum (TMAl,6N) were used as the metal-organic precursors for Ga and Al, respectively. High purity oxygen and argon (99.999%) were used as the O source and carrier gas. The growth temperature and growth pressure were set to about 750 °C and 20 torr.[19] We deposited a β-Ga_2O_3 film for 30 min, and continued to deposit a 30-min β-$(Al_{0.25}Ga_{0.75})_2O_3$ film on it as a passivation layer. The deposition rates of β-Ga_2O_3 and β-$(Al_{0.25}Ga_{0.75})_2O_3$ film were 10 nm/min and 5 nm/min, respectively. The Al composition in β-Ga_2O_3 set in this work is 25%, which is a commonly used ratio. Metal–semiconductor–metal (MSM) PDs ohmic electrodes were fabricated by a radio-frequency magnetron sputtering, in which Ti 30 nm/Au 80 nm square electrodes films (2×2 mm) were deposition on the β-Ga_2O_3 and β-$(Al_{0.25}Ga_{0.75})_2O_3/\beta$-$Ga_2O_3$ films. The effective irradiation area is 4 mm^2. The crystalline quality of the β-$(Al_{0.25}Ga_{0.75})_2O_3/\beta$-$Ga_2O_3$ films were characterized by high-resolution x-ray diffraction (HRXRD, Bruker D8 Discover), and surface morphology were displayed by a field emission scanning electron microscope (FESEM FEI Helios 600). The optical features were investigated by optical diffuse absorption spectra employing a Shimadzu UV-2600 spectrophotometer. Al compositions and β-$(Al_xGa_{1-x})_2O_3/\beta$-$Ga_2O_3$ film energy bandgaps were studied by a Thermo Fisher Scientific ESCALAB 250Xi x-ray photoelectron spectroscope (XPS) with Al K_α radiation source ($h = 1486.7$ eV). The Keithley 4200-SCS test system was used to characterize the photoelectric performance of the device and is equipped with 254 nm and 365 nm ultraviolet excitation light sources. A Thorlabs PM120VA power meter was used to record and calibrate the light intensity.[20]

3. Results and discussion

The XRD ω–2θ diffraction pattern shows that the film has diffraction peaks at $2\theta = 18.95°$, $2\theta = 38.44°$ and $2\theta = 59.08°$ corresponding to β-Ga_2O_3 and β-$(Al_{0.25}Ga_{0.75})_2O_3/\beta$-$Ga_2O_3$ films $(\bar{2}01)$ $(\bar{4}02)$ and $(\bar{6}03)$ reflections respectively in Fig. 1(a).[21,22] The calculation of Al composition by XRD is mainly based on Vegard's law.[11,12,21,23] We approximate that the material is affected by the Al composition in a linear distribution on the lattice constant.[6,18,24] Therefore, we can tell the Al mole fraction based on the peak position shift of the β-$(Al_{0.25}Ga_{0.75})_2O_3$ layer from reference peak position. For instance, for β-$(Al_{0.25}Ga_{0.75})_2O_3/\beta$-$Ga_2O_3$, the difference of angle θ of Al_2O_3 or β-Ga_2O_3 is $\Delta\theta_0$, the angle shift of β-$(Al_{0.25}Ga_{0.75})_2O_3$ from β-Ga_2O_3 is $\Delta\theta$, then the Al mole fraction can be given as $X = \Delta\theta/\Delta\theta_0$. The calculated Al component is 24.72%, which approximates our predicted component concentration. Figure 1(b) shows the Ga_2O_3 and β-$(Al_{0.25}Ga_{0.75})_2O_3/\beta$-$Ga_2O_3$ $(\bar{6}03)$ diffraction peak, which displays that the $(\bar{6}03)$ diffraction peak gradually shifts to a high angle with the merger of Al. This is attributed to the atomic radius of Al smaller than that of Ga, which causes the peak position to gradually shift to a high angle.[5]

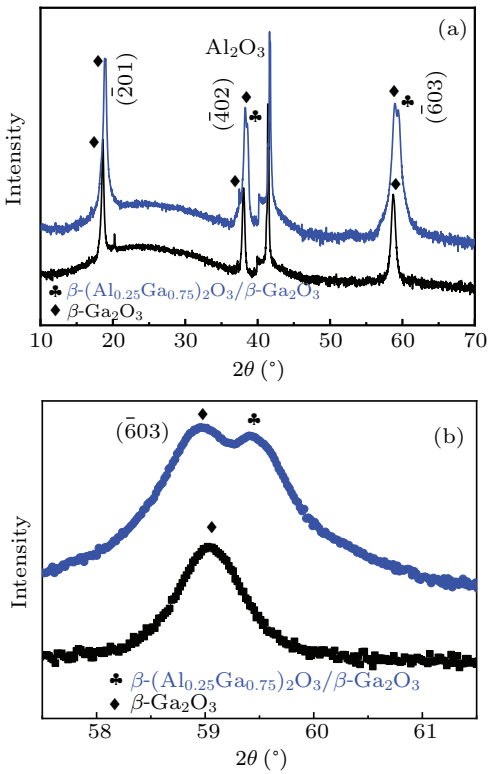


Fig. 1. (a) XRD pattern of the β-Ga_2O_3 and β-$(Al_{0.25}Ga_{0.75})_2O_3/\beta$-$Ga_2O_3$ films as grown by MOCVD. The observed $(\bar{2}01)$, $(\bar{4}02)$, $(\bar{6}03)$ diffraction peaks are located at 18.9°, 38.44° and 59.18°, respectively. (b) The $(\bar{6}03)$ diffraction peak of the β-Ga_2O_3 and β-$(Al_{0.25}Ga_{0.75})_2O_3/\beta$-$Ga_2O_3$ films.

Band gaps of the β-Ga_2O_3 and β-$(Al_{0.25}Ga_{0.75})_2O_3/\beta$-$Ga_2O_3$ films are calculated from the absorption spectrum measurements as shown in Fig. 2. With the increase of Al content, the absorption edge of the β-$(Al_{0.25}Ga_{0.75})_2O_3/\beta$-$Ga_2O_3$ film shifts to the direction of short wavelength. The inset in Fig. 2 shows the $(\alpha h\nu)^2$ of the film as a function of photo energy, with $h\nu$ representing the energy of the incident photon, α the absorption coefficient which is evaluated using the standard relation taking the film thickness into account.[25] The band gaps of the β-Ga_2O_3 and β-$(Al_{0.25}Ga_{0.75})_2O_3/\beta$-$Ga_2O_3$ films were evaluated by extrapolating the linear region to the horizontal axis, which were 4.99 eV and 5.07 eV, respectively. This indicates that the increase of Al component can cause a significant blue shift of the absorption edge which leads to an increase in the band gap.[26] Typical SEM images (5×5 μm^2) in Figs. 3(a) and 3(b) were taken for the β-Ga_2O_3 and β-$(Al_{0.25}Ga_{0.75})_2O_3/\beta$-$Ga_2O_3$ films. Although the addition of Al slightly affects the lattice constant of the β-Ga_2O_3 film, the images show that the β-$(Al_{0.25}Ga_{0.75})_2O_3/\beta$-$Ga_2O_3$ film keeps the compactness and flatness of the β-Ga_2O_3 film.

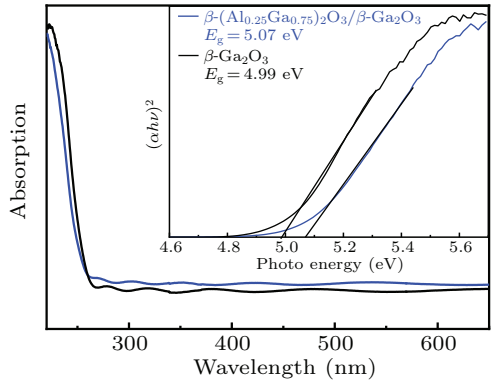


Fig. 2. Absorption spectra of the β-Ga_2O_3 and β-$(Al_{0.25}Ga_{0.75})_2O_3/\beta$-$Ga_2O_3$ films. The E_g of β-Ga_2O_3 and β-$(Al_{0.25}Ga_{0.75})_2O_3$/$Ga_2O_3$ films are given in the inset.

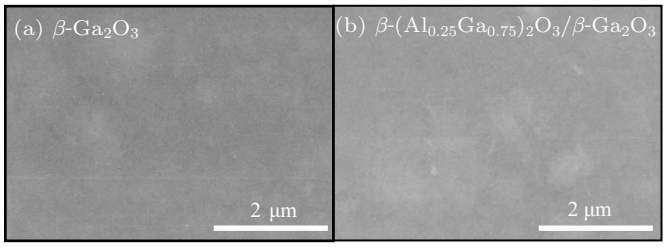


Fig. 3. The SEM images (scan area 2×2 μm^2): (a) β-Ga_2O_3, (b) β-$(Al_{0.25}Ga_{0.75})_2O_3/\beta$-$Ga_2O_3$.

X-ray photoelectron spectroscopy (XPS) tests on the β-Ga_2O_3 and β-$(Al_{0.25}Ga_{0.75})_2O_3/\beta$-$Ga_2O_3$ films are performed to verify the Al content and band gap verification. XPS is usually used to analyze the binding energy of nuclear-level electrons in materials.[5,22] Wide survey scans in the binding energy range of 0–1200 eV for the β-Ga_2O_3 and β-$(Al_{0.25}Ga_{0.75})_2O_3/\beta$-$Ga_2O_3$ films were performed as shown in Fig. 4(a). The XPS spectroscopy confirms the electron peak of Ga, Al, and O.[15] The peak position is regulated by C 1s of 284.6 eV. Compared to β-Ga_2O_3, the β-$(Al_{0.25}Ga_{0.75})_2O_3/\beta$-$Ga_2O_3$ film exhibits the obvious peak shift towards the higher binding energy. The insets in Figs. 4(b) and 4(c) show the high-resolution XPS spectra of Ga $2p_{3/2}$ and Al 2p core levels for the Ga_2O_3 and β-$(Al_{0.25}Ga_{0.75})_2O_3/\beta$-$Ga_2O_3$ films. From Fig. 4(b), Ga $2p_{3/2}$ core levels of the β-$(Al_{0.25}Ga_{0.75})_2O_3/\beta$-$Ga_2O_3$ films with different Al content are located at 1117.5 eV, which is attributed to the Ga–O bonding.[12,27] The peak intensity gradually increases with the increasing Al content, and no obvious shift is observed. Al 2p peaks of the β-$(Al_{0.25}Ga_{0.75})_2O_3/\beta$-$Ga_2O_3$ films are shown in Fig. 4(c). It is obvious that with the increasing Al content, the diffraction intensity becomes greater and no peaks are observed in the β-Ga_2O_3 film. This trend reflects the change in the ratio of Al/Ga atoms in the film. In order to verify the chemical state of the β-$(Al_{0.25}Ga_{0.75})_2O_3/\beta$-$Ga_2O_3$ film, O 1s was subjected to Gaussian fitting peak separation processing in Figs. 4(d) and 4(e). O_1 represents the oxygen atom located in the crystal lattice, and the binding energy is generally at 530.1 ± 0.1 eV;[15,19] O_2 usually represents oxygen vacancy defects (V_O) in the film and the binding energy is generally at 530.8 ± 0.1 eV.[27] The area of each peak can be used to indicate the concentration of the component, and the ratio of $O_2/(O_1+O_2)$ can be used to indicate the concentration of oxygen vacancy defects.[24,27] From Fig. 4(d), it can be seen that the concentration of oxygen vacancy defects decreases from 0.54 (β-Ga_2O_3) to 0.4 of β-$(Al_{0.25}Ga_{0.75})_2O_3/\beta$-$Ga_2O_3$. It shows that the Al composition within a certain content can offset the generation of oxygen vacancies, and obtain a low defect concentration in the β-$(Al_xGa_{1-x})_2O_3$ film.[12]

The β-Ga_2O_3 and β-$(Al_{0.25}Ga_{0.75})_2O_3/\beta$-$Ga_2O_3$ films were utilized to fabricate the MSM ultraviolet photodetector, the current–voltage (I–V) characteristics are measured under dark and 254 nm UV illumination (100 μW/cm) as shown in Fig. 5(a), which includes an inset of schematic diagram of the cross section. However, compared to the β-Ga_2O_3 devices, the β-$(Al_{0.25}Ga_{0.75})_2O_3/\beta$-$Ga_2O_3$ devices exhibit very low dark current, especially displayed 18 pA (at 5 V bias), which sharply reduces about 50 times. The reason from the analysis may be that the surface passivation of β-$(Al_{0.25}Ga_{0.75})_2O_3/\beta$-$Ga_2O_3$ reduces the surface state density of the device, surface leakage current decreases, and at the same time, β-$(Al_{0.25}Ga_{0.75})_2O_3$ acts as a high-resistance semi-insulating layer, which contributes significantly to the reduction of dark current.[28] In addition, it also benefits from the low oxygen vacancy density of the β-$(Al_{0.25}Ga_{0.75})_2O_3/\beta$-$Ga_2O_3$ epitaxial film. Such a low dark current results in an outstanding current on/off ratio, which is 2.16×10^5, better than 2.3 times that of the β-Ga_2O_3 devices. Figure 5(b) shows the switching characteristics (I–t curve) of the β-Ga_2O_3 and

β-$(Al_{0.25}Ga_{0.75})_2O_3/\beta$-$Ga_2O_3$ devices, meanwhile, the fitting result of the rise and fall times was displayed in Fig. 5(b) using the fitted equation $I = I_0 + Ae^{-t/\tau_1} + Be^{-t/\tau_2}$. It includes the fitting results at the rise time and fall time denoted by τ_r and τ_d, respectively.[24,29,30] From Fig. 5(b), all the samples show excellent switching characteristics, the PDs exhibit stable photo current after 4 illumination pulses with a light intensity of 100 μW/cm and a 5 V bias for 20 s. Under 5 V bias, τ_r/τ_d for the β-Ga_2O_3 and β-$(Al_{0.25}Ga_{0.75})_2O_3/\beta$-$Ga_2O_3$ devices are 5.30/0.09 s and 0.32/0.1 s, respectively. Extremely fast response time for the β-$(Al_{0.25}Ga_{0.75})_2O_3$ passivated devices, 16.56 times faster than the β-Ga_2O_3 devices.[15,31,32] To further evaluate the detection performance of each device in a comprehensive manner, Fig. 5(c) shows the responsivities R, detectivities D, and external quantum efficiency (EQE) of the Ga_2O_3 and β-$(Al_{0.25}Ga_{0.75})_2O_3/\beta$-$Ga_2O_3$ devices. Responsivities can be calculated by the following equation $R(\lambda) = (I_\lambda - I_d)/(P_\lambda S)$, in which $R(\lambda)$ is responsivity, I_λ is the UV-irradiated photocurrent, I_d is the dark current, P_λ and S represent the illumination power intensity and effective light area. The other two important PD parameters are obtained according to the formulas $D = (R \times S^{1/2})/(2eI_d)^{1/2}$ and EQE$= Rhc/e\lambda$, with h, c, and e being the Planck constant, the speed of light, and the charge of electron, respectively.[15,19,20,31,33] The calculated detectivities of the β-Ga_2O_3 and β-$(Al_{0.25}Ga_{0.75})_2O_3/\beta$-$Ga_2O_3$ devices are 3.49×10^{17} Jones and 9.26×10^{17} Jones, respectively. The detectivity of a passivated β-Ga_2O_3 detector on the surface is 2.65 times higher than that of a β-Ga_2O_3 device. Notably, the β-$(Al_{0.25}Ga_{0.75})_2O_3$ passivated device responsivity and EQE have different levels of optimization at bias 5 V and light intensity of 100 μW/cm, the responsivity is 2.8 A/W, and the EQE reaches 3.05×10^4%. Such a large EQE indicates that the PDs have a large gain, which may be the gain of avalanche.[26,34]

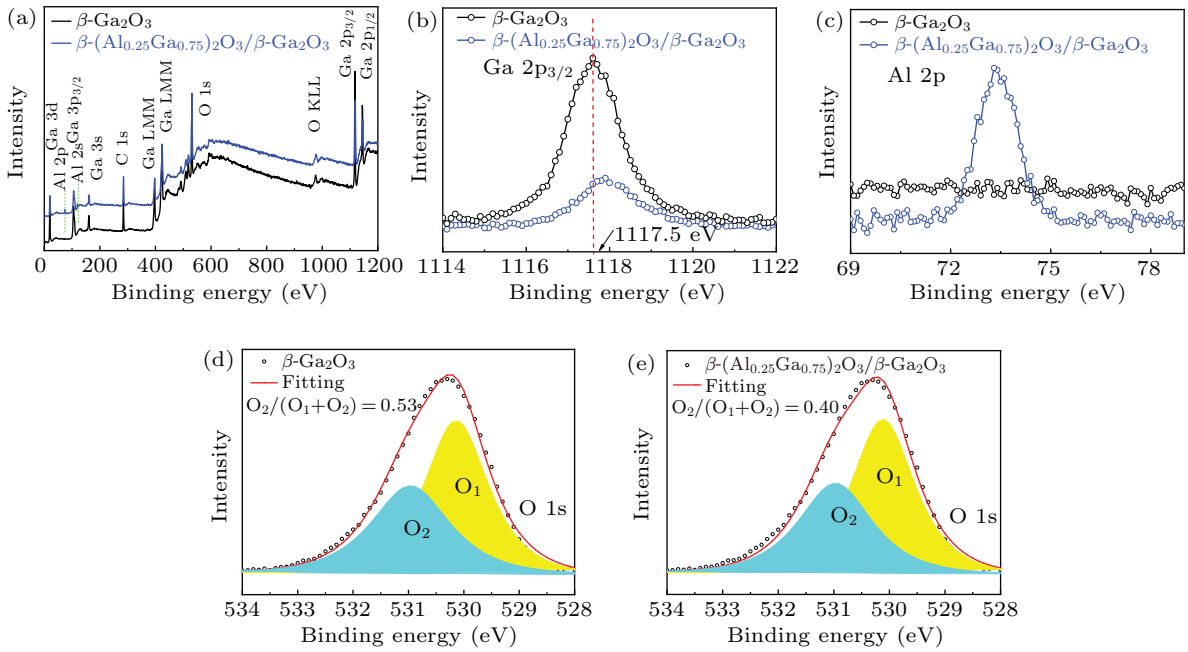


Fig. 4. XPS wide scan spectra (a), Ga $2p_{3/2}$ (b), Al 2p (c); (d)–(e) XPS spectra of O 1s of the β-Ga_2O_3 and β-$(Al_{0.25}Ga_{0.75})_2O_3/\beta$-$Ga_2O_3$ films.

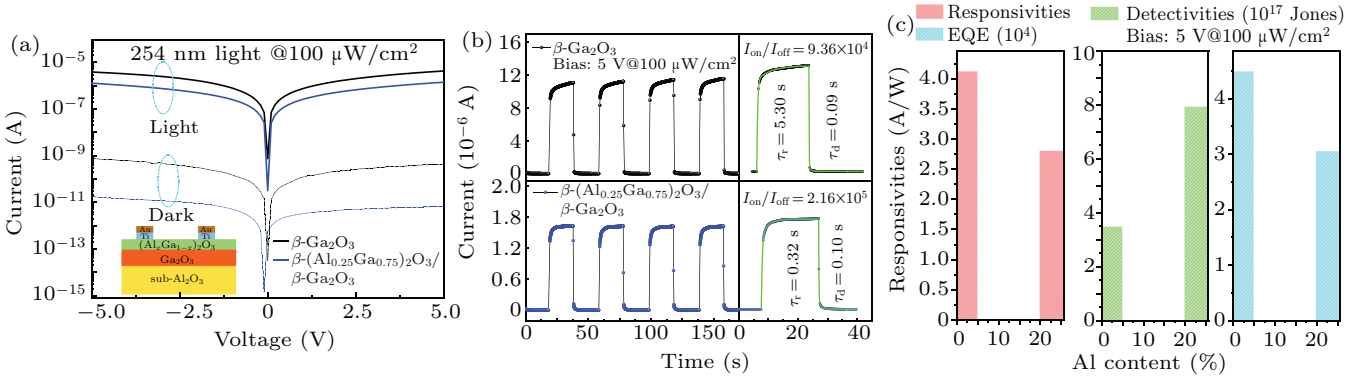


Fig. 5. (a) Logarithmic I–V characteristics of MSM photodetectors based on the β-Ga_2O_3 and β-$(Al_{0.25}Ga_{0.75})_2O_3/\beta$-$Ga_2O_3$ films under dark and light conditions. The inset gives a schematic diagram of the cross-sectional structure of the detector. (b) Logarithmic I–T at 5 V with 254-nm light on/off switching under 100 μW/cm^2 and the fitting response speeds for the Ga_2O_3 and β-$(Al_{0.25}Ga_{0.75})_2O_3/\beta$-$Ga_2O_3$ photodetectors. (c) Responsivity, detectivity, and EQE corresponding to devices of the β-Ga_2O_3 and β-$(Al_{0.25}Ga_{0.75})_2O_3/\beta$-$Ga_2O_3$ films.

Table 1. Performance comparison of different photodetectors based on the β-Ga_2O_3 films.

Material	Growth method	PDCR	EQE (%)	D^* (Jones)	R (mA/W)	Bias voltage (V)	References
β-Ga_2O_3	PLD	7.13×10^3		–	0.7	–	[37]
β-Ga_2O_3	MBE	10^2	18	–	37	10	[38]
β-Ga_2O_3		3.31×10^5		4.9×10^{11}	1050	–	[39]
βGa_2O_3	PLD	16.7		–	350	–	[40]
β-Ga_2O_3	MOCVD	104		–	1640	3	[41]
β-Ga_2O_3	MOCVD	9.36×10^4	3.05×10^4	3.49×10^{17}	2807	5	this work
β-$(Al_{0.25}Ga_{0.75})_2O_3/\beta$-$Ga_2O_3$	MOCVD	2.16×10^5	4.49×10^4	9.26×10^{17}	4120	5	this work

The comprehensive performance comparison with the recently reported β-Ga_2O_3 based PDs is shown in Table 1.[35,36] The results prove that the β-$(Al_{0.25}Ga_{0.75})_2O_3$ passivated devices provide a comparable outstanding optoelectronic performance, especially detectivities and external quantum effects compared to the β-Ga_2O_3 PDs.

To better understand the charge carrier transport mechanism of the β-$(Al_{0.25}Ga_{0.75})_2O_3$ passivated devices, the energy band alignment is shown in Fig. 6(a). The energy band position of the device was obtained based on previous reports and optical absorption analysis.[5] Figure 6(b) shows the energy band structure of the β-$(Al_{0.25}Ga_{0.75})_2O_3$ in the dark after contact with β-Ga_2O_3. After the β-$(Al_{0.25}Ga_{0.75})_2O_3$ passivation layer grows, the charge carriers keep flowing until the Fermi energy level is homogeneous and the carrier diffusion motion forms a space charge region at the heterogeneous interface, forming a depletion layer and a built-in electric field to maintain the drift and diffusion motion of the equilibrium electron and hole carriers. The highly resistive β-$(Al_{0.25}Ga_{0.75})_2O_3$ passivation layer grows with few free electrons at the interface and the defect states at the surface are covered, resulting in extremely low dark currents. However, under the UV irradiation at 254 nm, a large number of electron–hole pairs are generated, and the transport mechanism for carriers is greatly changed as shown in Fig. 6(c). When the photogenerated electron–hole pair drifts and diffuses into the built-in electric field, the electrons and holes are rapidly separated and converted into free carriers. The free electrons are transferred from the β-Ga_2O_3 to the β-$(Al_{0.25}Ga_{0.75})_2O_3$, and the holes are drifted from the β-$(Al_{0.25}Ga_{0.75})_2O_3$ to the β-Ga_2O_3 and collected at the Ti/Au electrode under the action of electric field.

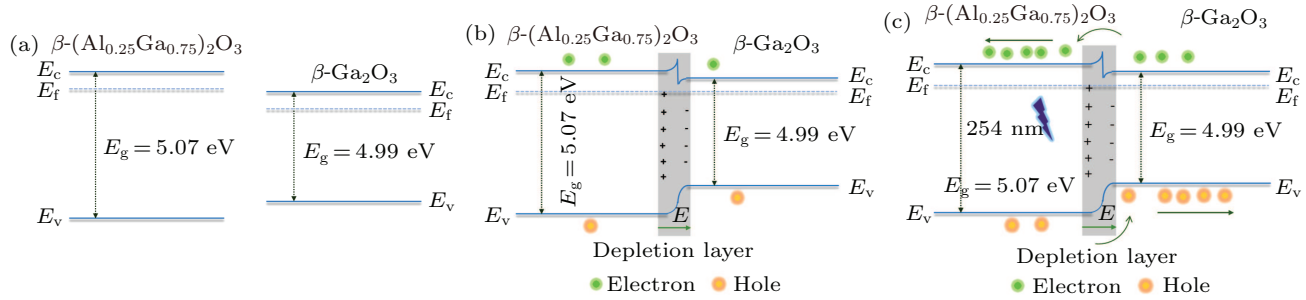


Fig. 6. The energy band alignment of the β-$(Al_{0.25}Ga_{0.75})_2O_3/\beta$-$Ga_2O_3$ heterojunction: (a) before contact, (b) after contact under dark state, (c) after contact under 254 nm illumination at 5 V.

4. Conclusion

In summary, we have compared the photodetection performances of two devices by growing an β-$(Al_{0.25}Ga_{0.75})_2O_3$ passivation layer on the surface of β-Ga_2O_3 films, and found that under the illumination with 254 nm light at bias 5 V, the β-$(Al_{0.25}Ga_{0.75})_2O_3$ passivated devices show low dark current and high current on/off ratio compared to the β-Ga_2O_3 devices. The dark current is sharply reduced by about 50 times after passivation of the β-Ga_2O_3 surface, and the current on/off ratio increases by approximately 2 times. This is attributed to the β-$(Al_{0.25}Ga_{0.75})_2O_3$ surface passivation, which reduces the surface trap state and the surface leakage current. Large and low defect densities in the epitaxial films are an influential factor. This result shows that β-$(Al_{0.25}Ga_{0.75})_2O_3$ exhibits high purity passivation effect and it has potential applications as a passivation material in the field of ultraviolet photoelectric detection.

Acknowledgements

Project supported by China Postdoctoral Science Foundation (Grant No. 042600055) and Research on Frontiers of Materials Science, Beijing Municipal Science and Technology Commission (Grant No. Z181100004418006).

References

[1] Pearton S J, Yang J, Cary P H, Ren F, Kim J, Tadjer M J and Mastro M A 2018 *Appl. Phys. Rev.* **5** 011301
[2] Yan Z Y, Li S, Liu Z, Liu W J, Qiao F, Li P G, Tang X, Li X H, Yue J Y, Guo Y F and Tang W H 2022 *IEEE J. Sel. Top. Quantum Electron.* **28** 3803208
[3] Liu X Z, Yue C, Xia C T and Zhang W L 2016 *Chin. Phys. B* **25** 017201

[4] Wang X, Wu Z P, Cui W, Zhi Y S, Li Z P, Li P G, Guo D Y and Tang W H 2019 *Chin. Phys. B* **28** 017305

[5] Cui S J, Mei Z X, Hou Y N, Chen Q S, Liang H L, Zhang Y H, Huo W X and Du X L 2018 *Chin. Phys. B* **27** 067301

[6] Zhang F, Saito K, Tanaka T, Nishio M, Arita M and Guo Q 2014 *Appl. Phys. Lett.* **105** 162107

[7] Chu X L, Liu Z, Zhi Y S, Liu Y Y, Zhang S H, Wu C, Gao A, Li P G, Guo D Y, Wu Z P and Tang W H 2021 *Chin. Phys. B* **30** 017302

[8] Wu Y L, Weng W Y, Chang S J, Huang Z D and Chiu C J 2012 *ECS Meet. Abstr.* **MA2012-01** 1614

[9] Qian L X, Wu Z H, Zhang Y Y, Lai P T, Liu X Z and Li Y R 2017 *ACS Photon.* **4** 2203

[10] Qin Y, Sun H, Long S, Tompa G S, Salagaj T, Dong H, He Q, Jian G, Liu Q, Lv H and Liu M 2019 *IEEE Electron Device Lett.* **40** 1475

[11] Anhar Uddin Bhuiyan A F M, Feng Z, Johnson J M, Chen Z, Huang H L, Hwang J and Zhao H 2019 *Appl. Phys. Lett.* **115** 120602

[12] Anhar Uddin Bhuiyan A F M, Feng Z, Johnson J M, Huang H L, Hwang J and Zhao H 2020 *Cryst. Growth Des.* **20** 6722

[13] Zhang Y, Joishi C, Xia Z, Brenner M, Lodha S and Rajan S 2018 *Appl. Phys. Lett.* **112** 233503

[14] Varley J B, Perron A, Lordi V, Wickramaratne D and Lyons J L 2020 *Appl. Phys. Lett.* **116** 172104

[15] Zhang F, Hu C, Arita M, Saito K, Tanaka T and Guo Q 2020 *AIP Adv.* **10** 065125

[16] Miller R, Alema F and Osinsky A 2018 *IEEE Trans. Semicond. Manuf.* **31** 467

[17] Uchida T, Jinno R, Takemoto S, Kaneko K and Fujita S 2018 *Jpn. J. Appl. Phys.* **57** 040314

[18] Ito H, Kaneko K and Fujita S 2012 *Jpn. J. Appl. Phys.* **51** 053102

[19] Li S, Yue J, Ji X, Lu C, Yan Z, Li P, Guo D, Wu Z and Tang W 2021 *J. Mater. Chem. C* **9** 5437

[20] Li S, Zhi Y, Lu C, Wu C, Yan Z, Liu Z, Yang J, Chu X, Guo D, Li P, Wu Z and Tang W 2021 *J. Phys. Chem. Lett.* **12** 447

[21] Zhao Z, Zhao H, Ako R T, Nickl S, and Sriram S 2020 *Appl. Phys. Lett.* **117** 011105

[22] Ji X, Yue J, Qi X, Meng D, Chen Z and Li P 2021 *J. Appl. Phys.* **130** 075301

[23] Bhuiyan A F M A U, Feng Z, Johnson J M, Huang H L, Sarker J, Zhu M, Karim M R, Mazumder B, Hwang J and Zhao H 2020 *APL Mater.* **8** 031104

[24] Krueger B W, Dandeneau C S, Nelson E M, Dunham S T, Ohuchi F S and Olmstead M A 2016 *J. Am. Ceram. Soc.* **99** 2467

[25] Jiao S, Lu H, Wang X, Nie Y, Wang D, Gao S and Wang J 2019 *ECS J. Solid State Sci. Technol.* **8** Q3086

[26] Feng Q, Li X, Han G, Huang L, Li F, Tang W, Zhang J and Hao Y 2017 *Opt. Mater. Express* **7** 1240

[27] Wang J, Xiong Y, Ye L, Li W, Qin G, Ruan H, Zhang H, Fang L, Kong C and Li H 2021 *Opt. Mater.* **112** 110808

[28] Chen X, Xia N, Yang Z, Gong F, Wei Z, Wang D, Tang J, Fang X, Fang D and Liao L 2018 *Nanotechnology* **29** 095201

[29] Oshima T, Kato Y, Kawano N, Kuramata A, Yamakoshi S, Fujita S, Oishi T and Kasu M 2017 *Appl. Phys. Express* **10** 035701

[30] Zhang D, Lin W, Liu S, Zhu Y, Lin R, Zheng W and Huang F 2019 *ACS Appl. Mater. Interfaces* **11** 48071

[31] Ravadgar P, Horng R H, Yao S D, Lee H Y, Wu B R, Ou S L and Tu L W 2013 *Opt. Express* **21** 24599

[32] Chu X L, Liu Z, Zhi Y S, Liu Y Y, Zhang S H, Wu C, Gao A, Li P G, Guo D Y, Wu Z P and Tang W H 2021 *Chin. Phys. B* **30** 017302

[33] Li S, Guo D, Li P, Wang X, Wang Y, Yan Z, Liu Z, Zhi Y, Huang Y, Wu Z and Tang W 2019 *ACS Appl. Mater. Interfaces* **11** 35105

[34] Hu G C, Shan C X, Zhang N, Jiang M M, Wang S P and Shen D Z 2015 *Opt. Express* **23** 13554

[35] Li Y, Zhang D, Jia L, Zhu S, Zhu Y, Zheng W and Huang F 2021 *Sci. China Mater.* **64** 3027

[36] Liu Z, Zhi Y S, Zhang M L, Yang L L, Li S, Yan Z Y, Zhang S H, Guo D Y, Li P G, Guo Y F and Tang W H 2022 *Chin. Phys. B* **31** 088503

[37] Tak B R, Garg M, Dewan S, Torres-Castanedo C G, Li K H, Gupta V, Li X and Singh R 2019 *J. Appl. Phys.* **125** 144501

[38] Oshima T, Okuno T and Fujita S 2007 *Jpn. J. Appl. Phys.* **46** 7217

[39] Ma M, Zhang D, Li Y, Lin R, Zheng W and Huang F 2019 *ACS Appl. Electron. Mater.* **1** 1653

[40] Guo D Y, Shi H Z, Qian Y P, Lv M, Li P G, Su Y L, Liu Q, Chen K, Wang S L, Cui C, Li C R and Tang W H 2017 *Semicond. Sci. Technol.* **32** 03LT01

[41] Li Y, Zhang D, Lin R, Zhang Z, Zheng W and Huang F 2019 *ACS Appl. Mater. Interfaces* **11** 1013